

LA-UR-18-20542 (Accepted Manuscript)

Ultrahigh-resolution neutron spectroscopy of low-energy spin dynamics in UGe₂

Halsbeck, Franz; Saeubert, Steffen; Seifert, Marc; Franz, Christian; Schulz, Michael; Heinemann, Andre; Keller, Thomas; Das, Pinaki; Thompson, Joe D; Bauer, Eric D; Pfleiderer, Christian; Janoschek, Marc

Provided by the author(s) and the Los Alamos National Laboratory (2019-04-10).

To be published in: Physical Review B

DOI to publisher's version: 10.1103/PhysRevB.99.014429

Permalink to record: <http://permalink.lanl.gov/object/view?what=info:lanl-repo/lareport/LA-UR-18-20542>

Disclaimer:

Los Alamos National Laboratory, an affirmative action/equal opportunity employer, is operated by Triad National Security, LLC for the National Nuclear Security Administration of U.S. Department of Energy under contract 89233218CNA000001. By approving this article, the publisher recognizes that the U.S. Government retains nonexclusive, royalty-free license to publish or reproduce the published form of this contribution, or to allow others to do so, for U.S. Government purposes. Los Alamos National Laboratory requests that the publisher identify this article as work performed under the auspices of the U.S. Department of Energy. Los Alamos National Laboratory strongly supports academic freedom and a researcher's right to publish; as an institution, however, the Laboratory does not endorse the viewpoint of a publication or guarantee its technical correctness.

Ultra-High Resolution Neutron Spectroscopy of Low-Energy Spin Dynamics in UGe₂

F. Haslbeck,^{1,2} S. Säubert,^{1,3} M. Seifert,^{1,3} C. Franz,³ M. Schulz,³ A. Heinemann,⁴ T. Keller,^{5,6} Pinaki Das,^{7,*} J. D. Thompson,⁷ E. D. Bauer,⁷ C. Pfleiderer,¹ and M. Janoschek^{2,7,8,†}

¹Physik-Department, Technische Universität München, D-85748 Garching, Germany

²Institute for Advanced Study, Technische Universität München, D-85748 Garching, Germany

³Heinz Maier-Leibnitz Zentrum Garching, Technische Universität München, D-85748 Garching, Germany

⁴German Engineering Materials Science Centre (GEMS) at Heinz Maier-Leibnitz Zentrum (MLZ),

Helmholtz-Zentrum Geesthacht GmbH, D-85747 Garching, Germany

⁵Max-Planck-Institut für Festkörperforschung, D-70569 Stuttgart, Germany

⁶Max Planck Society Outstation at the Forschungsneutronenquelle Heinz Maier-Leibnitz (MLZ), D-85747 Garching, Germany

⁷Los Alamos National Laboratory, Los Alamos, New Mexico 87545, USA

⁸Laboratory for Scientific Developments and Novel Materials, Paul Scherrer Institut, Villigen PSI, Switzerland

(Dated: December 20, 2018)

Studying the prototypical ferromagnetic superconductor UGe₂ we demonstrate the potential of the Modulated Intensity by Zero Effort (MIEZE) technique—a novel neutron spectroscopy method with ultra-high energy resolution of at least 1 μeV —for the study of quantum matter. We reveal purely longitudinal spin fluctuations in UGe₂ with a dual nature arising from $5f$ electrons that are hybridized with the conduction electrons. Local spin fluctuations are perfectly described by the Ising universality class in three dimensions, whereas itinerant spin fluctuations occur over length scales comparable to the superconducting coherence length, showing that MIEZE is able to spectroscopically disentangle the complex low-energy behavior characteristic of quantum materials.

Ultra-slow spin dynamics represent a key characteristic of quantum matter such as quantum spin liquids¹, electronic nematic phases², topological spin textures^{4,5}, non-Fermi liquid behavior³, and unconventional superconductivity⁶⁻⁹. For the clarification of these phenomena spectroscopic methods with excellent momentum and energy resolution are required, as key characteristics emerge typically in the low milli-Kelvin range. In principle, neutron scattering is ideally suited for studies of the relevant spin excitations. However, the typical energy resolution of conventional neutron spectroscopy corresponds to Kelvin temperatures. Although techniques such as neutron spin-echo spectroscopy offer ultra-high resolution of sub- μeV , they are incompatible with conditions that depolarize neutron beams such as ferromagnetism (FM), superconductivity or large magnetic fields.

The discovery of superconductivity in the FM state of UGe₂ highlights the combination of scientific and experimental challenges that arise in the study of the complex low-energy behavior of quantum matter that characteristically emerges due to the competition of high-energy atomic energy scales¹⁰. Namely, actinide-based compounds such as UGe₂ are formidable model systems, where the hybridization of itinerant d and localized f electrons drives low-energy excitations that mediate a multitude of novel states¹¹⁻¹³. Traditionally the concomitant subtle reconstruction of the electronic structure has been studied via the charge channel, which fails to provide the required high resolution^{14,15}. Exploiting in contrast the spin channel recent advances in neutron spectroscopy provided new insights¹⁶⁻¹⁸.

Using an implementation of neutron resonance spin echo (NRSE) spectroscopy that is insensitive to depolarizing conditions, namely the so-called Modulated Intensity by Zero Effort (MIEZE)¹⁹, we report a study of UGe₂ in which we identify the enigmatic low-energy excitations as an unusual combination of fluctuations attributed normally either to itinerant or localized electrons in an energy and momentum range com-

parable to the superconducting coherence length and ordering temperature. As the superconductivity in UGe₂ represents a prototypical form of quantum matter, our study underscores also the great potential of the MIEZE technique in studies of quantum matter on a more general note.

At ambient pressure UGe₂ displays ferromagnetism with a large Curie temperature, $T_c = 53$ K, and a large ordered moment, $\mu_{\text{FM1}} = 1.2 \mu_{\text{B}}(\text{FM1})$ ^{20,21}. Under increasing pressure FM order destabilizes, accompanied by the emergence of a second FM phase below $T_x < T_c$ where $\mu_{\text{FM2}} = 1.5 \mu_{\text{B}}(\text{FM2})$. The FM2 and FM1 phases vanish discontinuously at $p_x \approx 12.2$ kbar and $p_c \approx 15.8$ kbar, respectively²¹, while superconductivity emerges between ≈ 9 kbar $< p_x$ and p_c . Evidence for a microscopic coexistence of FM order and superconductivity makes UGe₂ a candidate for p-wave pairing, where the Cooper pairs form spin triplets²⁰. This p-wave superconductivity is believed to be mediated by an abundance of low-lying longitudinal spin fluctuations associated with a FM quantum phase transition (QPT), where transverse spin fluctuations are theoretically known to break spin-triplet pairing²². Neutron triple-axis spectroscopy (TAS) at ambient pressure indeed identified predominantly longitudinal spin fluctuations in UGe₂²³, but failed to provide insights into the character of the fluctuations in the momentum and energy range comparable to the superconducting coherence length and transition temperature, respectively.

Prior to our study the interplay of seemingly conflicting ingredients of the spectrum of spin fluctuations were unresolved. On the one hand, the strong Ising anisotropy promotes longitudinal spin fluctuations as typically attributed to localized electrons in the presence of strong to spin-orbit coupling. This is contrasted, on the other hand, by the notion of Cooper pairs and a well developed, strongly exchange-split Fermi surface^{22,24}. Consistent with this dichotomy characteristic of p-wave superconductivity, our ultra-high resolution data reveals that the low-energy spin fluctuations of UGe₂ reflect a subtle

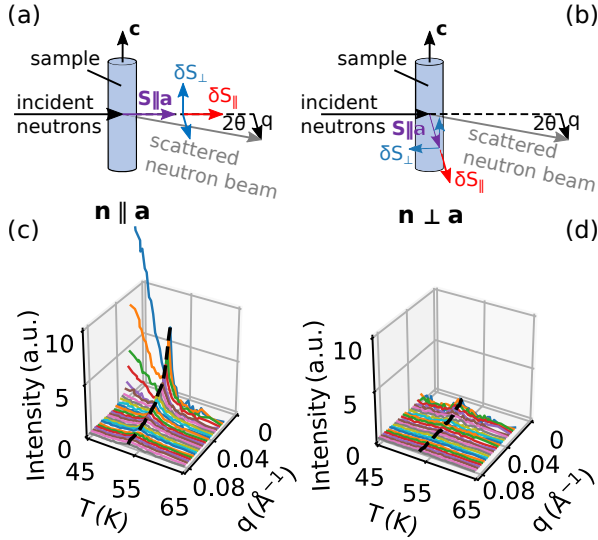


FIG. 1. Magnetic intensity in UGe_2 near the Curie temperature $T_C = 52.7$ K. (a) and (b) show two experimental configurations with the a axis parallel or perpendicular to the incident neutron beam \mathbf{n} , respectively, used to differentiate longitudinal from transverse spin fluctuations (see text). (c) and (d) show the observed energy-integrated intensities for $\mathbf{n} \parallel a$ and $\mathbf{n} \perp a$ as a function of temperature T and momentum transfer \mathbf{q} . The black dashed line marks T_C .

interplay of itinerant and local electronic degrees of freedom on scales comparable to the superconductivity.

NRSE achieves extreme energy resolution by encoding the energy transfer $\hbar\omega$ of the neutrons in their polarization as opposed to a change of wavelength. However, FM domains, Meissner flux expulsion or applied magnetic fields typically depolarize the beam. We used therefore a novel NRSE technique, so called MIEZE, implemented at the instrument RESEDA at the Heinz Heinz Maier-Leibnitz Zentrum (MLZ)^{25–27}. Generating an intensity modulated beam by means of resonant spin flippers and a spin analyzer in front of the sample the amplitude of the intensity modulation assumes the role of the NRSE polarization. Because all spin manipulations are performed before the sample, beam depolarizing effects are no longer important. Using incident neutrons with a wavelength $\lambda = 6$ Å and $\Delta\lambda/\lambda \approx 10\%$ provided by a velocity selector, we achieved an energy resolution of $\Delta E \approx 1 \mu\text{eV}$. MIEZE in small angle neutron scattering (SANS) configuration also provides high momentum \mathbf{q} resolution of approximately 0.015 Å⁻¹. The MIEZE setup is described in the supplemental material²⁸.

A high-quality single crystal of UGe_2 was grown by the Czochralski technique followed by an annealing similar to Ref. 29. A cylindrical piece with nearly constant diameter of 7 mm and 16 mm length ($m = 6$ g) with the crystallographic c axis approximately parallel to the cylinder axis was cut for the MIEZE experiments. The sample was oriented using neutron Laue diffraction so that c was perpendicular to the scattering plane. The Laue images also confirm a high-quality single-

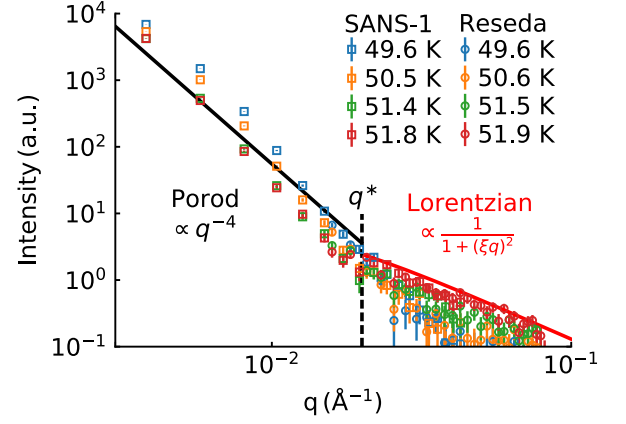


FIG. 2. \mathbf{q} -dependence of the intensity for selected T below T_C for $\mathbf{n} \parallel a$. Below $q^* \approx 0.02$ Å⁻¹ the intensity is well described by Porod scattering due to ferromagnetic (FM) domains (black solid line), whereas above q^* a Lorentzian shape due to critical spin fluctuations is observed (red solid line).

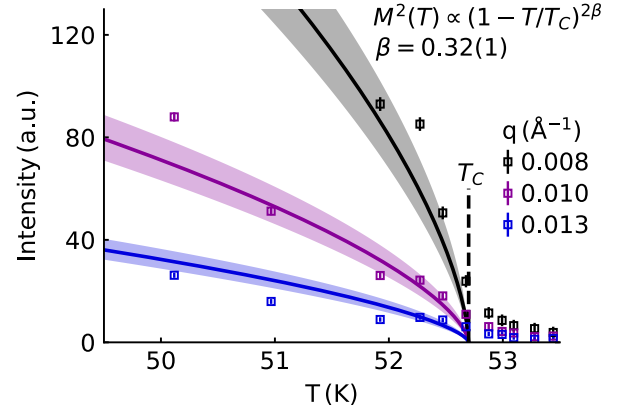


FIG. 3. The T dependence of the Porod scattering for $q < q^*$ follows the FM order parameter M via $M^2(T) \propto (1 - T/T_C)^{2\beta}$ with $\beta = 0.32(1)$ (solid lines). The shaded regions denote the uncertainty of the fit of β .

grain sample²⁸. Neutron depolarization imaging measurements²⁸ of the same sample reveal that the magnetic properties of the crystal are completely homogeneous with a Curie temperature $T_C = 52.68(3)$ K demonstrating that this sample is optimal for the investigation of critical spin fluctuations. Magnetic susceptibility measurements were performed on a small piece ($m = 36$ mg) of the same sample in a Quantum Design magnetic property measurement system (MPMS).

The magnetic cross-section is related to the imaginary part of the dynamical magnetic susceptibility $\chi''_{ij}(\mathbf{Q}, \omega)$ via

$$\frac{d^2\sigma}{d\Omega d\omega} \propto \frac{k_0}{k_f} (\delta_{ij} - \hat{q}_i \hat{q}_j) |F_{\mathbf{q}}|^2 [n(\omega) + 1] \chi''_{ij}(\mathbf{q}, \omega), \quad (1)$$

where k_0 and k_f are the wave vector of the incident and scat-

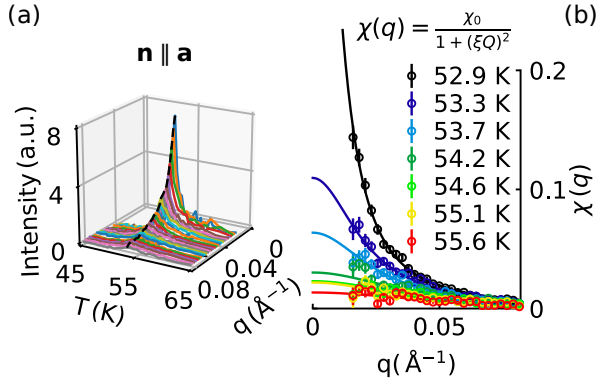


FIG. 4. (a) Temperature T and momentum transfer \mathbf{q} dependence of the critical Ising spin fluctuations in UGe_2 . (b) q -dependence of the magnetic susceptibility $\chi(q)$. Solid lines are fits to Eq. 3.

tered neutrons, respectively. \hat{q} is a unit vector parallel to the scattering vector \mathbf{q} and $n(\omega)$ is the Bose function. $F_{\mathbf{q}}$ is the uranium magnetic form factor.

In Fig. 1 we show the temperature and \mathbf{q} dependence of the energy-integrated intensity of the spin fluctuations in UGe_2 that was obtained by switching the MIEZE setup off. Non-magnetic background scattering obtained well above T_C was subtracted from all data sets shown. The temperature scan was carried out with the crystallographic a -axis, which is the magnetic easy-axis for UGe_2 oriented parallel ($\mathbf{n} \parallel a$) and perpendicular ($\mathbf{n} \perp a$) to the incident neutron beam, respectively. Due to the term $\delta_{ij} - \hat{q}_i \hat{q}_j$ in Eq. 1 neutron scattering is only sensitive to spin fluctuations that are perpendicular to \mathbf{q} . Because in SANS configuration \mathbf{q} is approximately perpendicular to the incident neutron beam, this allows to separate longitudinal (δS_{\parallel}) from transverse spin fluctuations (δS_{\perp}) as illustrated in Figs. 1(a) and (b). For $\mathbf{n} \parallel a$ both δS_{\parallel} and δS_{\perp} are perpendicular to \mathbf{q} . As shown in Fig. 1(c) substantial magnetic intensity is observed for this configuration. In contrast, for $\mathbf{n} \perp a$ only δS_{\perp} is perpendicular to \mathbf{q} and the vanishingly small signal observed in this case [see 1(d)] can only come from transverse spin fluctuations. Because of the cylindrical shape of the sample differences in neutron transmission between the two orientations are negligible. As shown in the supplemental material²⁸, the small intensity observed for $\mathbf{n} \perp a$ arises from finite \mathbf{q} resolution, demonstrating that the critical spin fluctuations in UGe_2 are solely longitudinal.

Inspecting the temperature dependence of the integrated intensity for $\mathbf{n} \parallel a$ [see Fig. 1(c)], a pronounced peak is centered at $T_C = 52.7$ K due to the divergence of critical spin fluctuations. For low q and for $T < T_C$ additional intensity is observed that increases like a magnetic order parameter. Fig. 2 shows the q -dependence of the intensity for a few temperatures below T_C . Below $q^* \approx 0.02 \text{ \AA}^{-1}$ the intensity is well-described by a q^{-4} dependence that is characteristic for scattering from FM domains that form below T_C ^{30,31}. To follow this so-called Porod scattering towards lower q , we have performed a supporting SANS experiment on the instrument SANS-1 at MLZ (details are described in²⁸) denoted

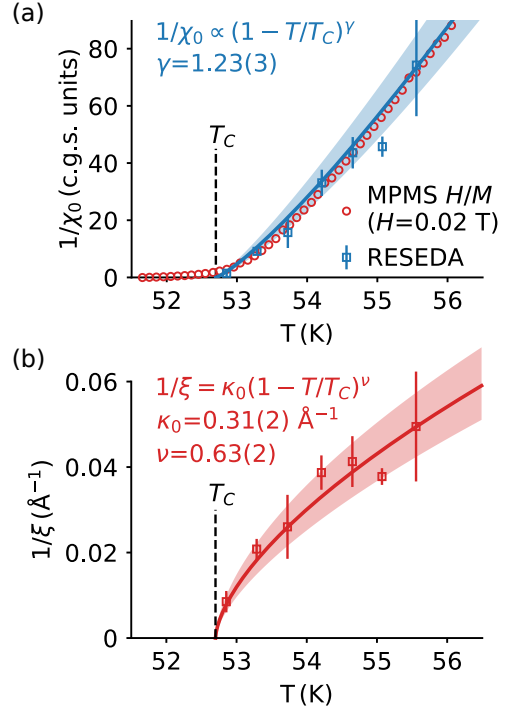


FIG. 5. The inverse susceptibility $1/\chi_0$ and inverse correlation length $1/\xi$ as a function of temperature T (near the Curie temperature $T_C = 52.7$ K), respectively, resulting from fits in Fig. 4. The blue squares in (a) denote the static easy-axis magnetic susceptibility H/M determined with a magnetic field $H = 0.1$ T. The solid black and red lines are fits to determine the critical exponents for χ_0 and ξ (see text), and the shaded region denotes the uncertainty of the fit.

with square symbols in Fig. 2. Observation of Porod scattering down to $q_{\min} = 0.004 \text{ \AA}^{-1}$ implies the onset of long-range order over length scales $\gg 2\pi/q_{\min} \approx 1600 \text{ \AA}$). In Fig. 3, we show the temperature dependence of the intensity for selected q below q^* . Near to T_C it evolves as $M^2(T) \propto (1 - T/T_C)^{2\beta}$. We find that $\beta = 0.32(1)$ describes our data perfectly in agreement with $\beta^{\text{theo}} = 0.32$ for a three-dimensional (3D) Ising system³². This is also in good agreement with $\beta = 0.36(1)$ from neutron diffraction³³.

For $q \geq q^*$ and for $T \approx T_C$ the q -dependence is described by a Lorentzian line shape characteristic of critical spin fluctuations with a correlation length ξ . The corresponding dynamical magnetic susceptibility is

$$\frac{\chi''(\mathbf{q}, \omega)}{\omega} = \chi(\mathbf{q}) \frac{\Gamma_q}{\Gamma_q^2 + \omega^2} \quad (2)$$

$$\chi(\mathbf{q}) = \frac{\chi_0}{1 + (\xi q)^2}, \quad (3)$$

where Γ_q and χ_0 are the momentum dependent relaxation frequency and the static magnetic susceptibility, respectively. Because of the longitudinal character of the spin fluctuations only χ''_{aa} is non-zero, and we have thus dropped the indices i, j . To investigate the critical scattering quantitatively, we subtract the Porod scattering [Fig. 2] from the observed inten-

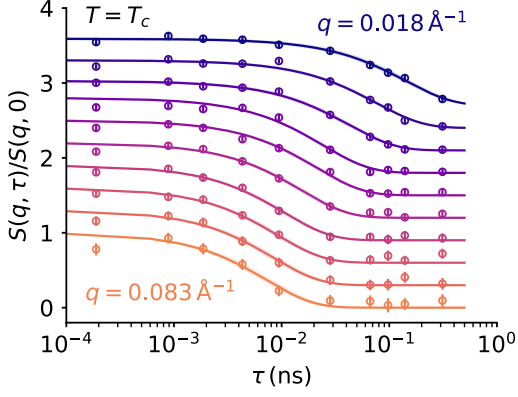


FIG. 6. Spin fluctuation spectrum of UGe₂ obtained by MIEZE. The intermediate scattering function $S(q, \tau)$ normalized to $S(q, 0)$ (static signal) is shown at $T_C = 52.7$ K for a range of momentum transfers q . Solid lines are fits to Eq. 4.

ities [Fig. 1(c)]. For our experimental conditions the quasi-static approximation is valid and thus integrating Eq. 1 with respect to $\hbar\omega$, we obtain $\frac{d\sigma}{d\Omega} \propto T\chi(\mathbf{q})$ (see supplemental material²⁸). We show $\chi(\mathbf{q})$ obtained by dividing the observed intensity by T for various temperatures in Fig. 4(b). The solid lines are fits to Eq. 3 to extract the T -dependence of χ_0 and ξ shown in Figs. 5(a) and (b), respectively. For comparison we show the static magnetic susceptibility H/M determined by bulk magnetization measurements in Fig. 5(a) (blue squares) that scales perfectly with χ_0 .

We find that $1/\chi_0 \propto (1 - T/T_C)^\gamma$ with $\gamma = 1.23(3)$ and $1/\xi = \kappa = \kappa_0(1 - T/T_C)^\nu$ with $\kappa_0 = 0.31(2)\text{\AA}^{-1}$ and $\nu = 0.63(2)$ [solid lines Figs. 5(a) and (b)]. The critical exponents are in excellent agreement with a 3D Ising FM, for which $\gamma^{\text{theo}} = 1.24$ and $\nu^{\text{theo}} = 0.63$ ³². Huxley *et al.* found $\kappa_0 = 0.29\text{\AA}^{-1}$ in good agreement with our result. In contrast, they determined $\nu = 1/2$, consistent with a mean-field transition²³. However, their study was limited to $q > 0.03\text{\AA}^{-1}$ and underestimate the divergence of the critical fluctuations.

We now discuss the results of our MIEZE measurements. MIEZE measures the intermediate scattering function $S(q, \tau)$ that is the time Fourier transform of the scattering function $S(q, \omega) = 1/\pi[n(\omega) + 1]\chi''_{ij}(\mathbf{q}, \omega)$ (cf. Eq. 1). In Fig. 6 we show $S(q, \tau)$ for various q at T_C . $S(q, \tau)$ for all other measured temperatures are shown in Ref. 28. Because the spin fluctuations have Lorentzian lineshape (see Eq. 2) we fit $S(q, \tau)$ with an exponential decay [solid lines in Fig. 6]:

$$S(q, \tau) = \exp(-|\Gamma_q| \cdot \tau). \quad (4)$$

The resulting fluctuation frequency Γ_q is shown in Fig. 7.

The momentum dependence of Γ_q is described by the dynamical exponent z via $\Gamma_q \propto q^z$. For $T \leq T_C$, we find that Γ_q is fitted perfectly by $z = 2.0(1)$ [Fig. 7(a)]. This is in excellent agreement with predictions for a 3D Ising FM, for which $z^{\text{theo}} = 2$ ³². For $T > T_C$, Γ_q is also well described by $z = 2$, however, only above a crossover value of $q^0 = 0.04\text{\AA}^{-1}$. Below q^0 , our data is best fit by $\Gamma_q = Aq^z$

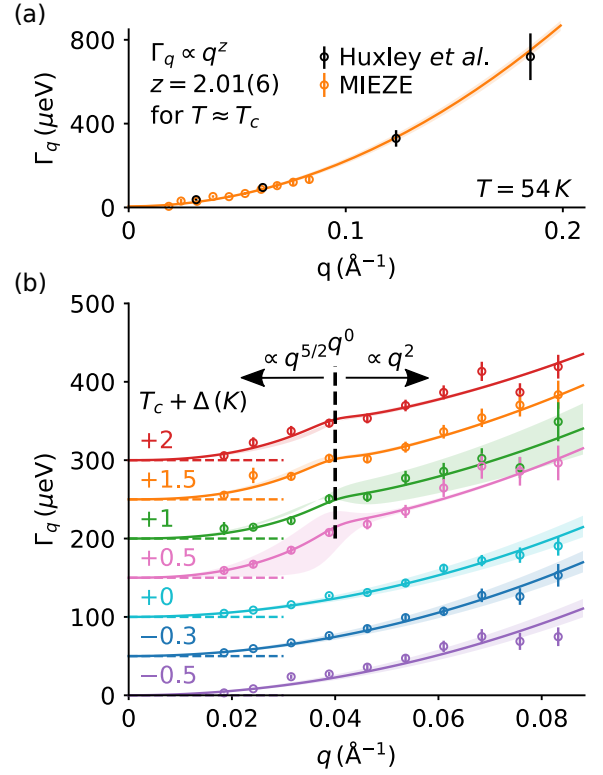


FIG. 7. The fluctuation frequency Γ_q of UGe₂ at various temperatures T as determined by fits of 4 to the data shown in Fig. 6. Solid lines are fits to $\Gamma_q \propto q^z$, where z is the dynamical critical exponent. (a) Comparison of our data to the high- q data by Huxley *et al.*²³ is shown. (b) We find two distinct regimes with $z = 2.5$ and 2 below and above $q^0 = 0.038\text{\AA}^{-1}$, respectively (see text). Data sets are shifted by $50\text{ }\mu\text{eV}$ for better readability as indicated by the horizontal dashed lines.

with $z = 2.53(4)$ (see Fig. 7). This is consistent with $z = 5/2$ calculated for itinerant FMs within critical renormalization group theory³⁶ and confirmed for various d -electron FMs such as Fe³⁷, Ni³⁸ and Co³⁹. Notably, typical values reported for A are $3\text{-}350\text{ meV}\text{\AA}^{5/237-40}$ consistent with $A=200(2)\text{ meV}\text{\AA}^{5/2}$ that we find for UGe₂. As demonstrated in the Fig. 7(a) for $T = 54$ K, the fit of Γ_q with $z = 2.0(1)$ also describes the data of Huxley *et al.*²³ (black empty circles) perfectly. However, they conclude that Γ_q remains finite for $q \rightarrow 0$ in contrast to our findings. This discrepancy is easily explained by considering that their experiment was limited to $q \geq 0.03\text{\AA}^{-1}$, which is only slightly below q^0 where we observe the crossover to $z = 5/2$.

Fig. 8 shows the T -dependence of Γ_q . For finite q , it follows the T -dependence of ξ via $\Gamma_q \propto (1/\xi)^z = (1 - T/T_C)^{z\nu}$ in agreement with the dynamical scaling prediction⁴¹. In Fig. 8(a) we show that for $q = 0.06\text{\AA}^{-1}$ both the results from Ref. 23 and our own are consistent with $z = 2$. Below q^0 , $z = 5/2$ agrees well with our data (solid line) consistent with the fits of Γ_q shown in Fig. 7.

For clean itinerant FMs the fluctuation spectrum is characterized by Landau damping as has been demonstrated for $3d$

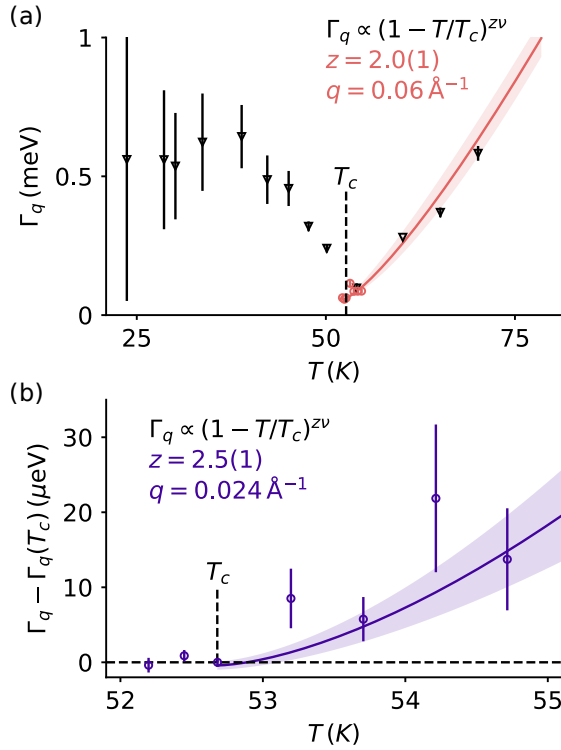


FIG. 8. Temperature(T)-dependence of the fluctuation frequency Γ_q for q above (a) and below (b) q^0 . (a) Comparison to data of Ref 23. Solid lines denote $\Gamma_q \propto (1 - T/T_c)^{2\nu}$ (see text).

transition metal materials^{42,43}. Here the product of the magnetic susceptibility with the fluctuation frequency, $\chi(q)\Gamma_q$, is given by the Lindhard dependence $(2/\pi)v_F\chi_Pq$ for $T > T_C$, where v_F and χ_P are the Fermi velocity and the non-interacting Pauli susceptibility, respectively^{44,45}. We show $\chi(q)\Gamma_q$ for UGe₂ in Fig. 9. Huxley *et al.*²³ who carried out measurements for $q \geq 0.03 \text{ \AA}^{-1}$ found that $\chi(q)\Gamma_q$ only weakly depends on q and concluded that it remains finite for $q \rightarrow 0$ [solid black line in Fig. 9]. This difference with respect to prototypical $3d$ electron itinerant FMs is likely due to strong spin-orbit coupling that modifies the spin fluctuation spectrum. Our data agrees with the weak q dependence above q^0 but clearly shows that $\chi(q)\Gamma_q \rightarrow 0$ for $q \rightarrow 0$, implying that the uniform magnetization is a conserved quantity in UGe₂. Our data is consistent with $\chi(q)\Gamma_q \propto q^{5/2}$ [solid blue line in Fig. 9]. This more pronounced q -dependence is expected by theory near T_C ⁴⁵, and agrees with $\Gamma_q \propto q^{5/2}$. Here, we highlight that although the q -range over which q^z with $z = 5/2$ is observed is limited, this behavior is corroborated via three independent methods that are illustrated in Figs. 7-9.

Our results demonstrate that the spin fluctuations in UGe₂ exhibit a dual character associated with localized $5f$ electrons that are hybridized with itinerant d electrons. Notably, as expected for a local moment FM with substantial uniaxial magnetic anisotropy all critical exponents determined from our results are in perfect agreement with the 3D Ising universality

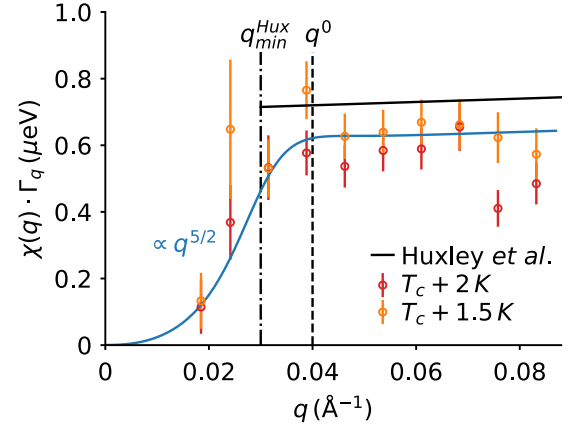


FIG. 9. Temperature(T)-dependence of the product of the magnetic susceptibility with the fluctuation frequency, $\chi(q)\Gamma_q$. The black line is $\chi(q)\Gamma_q$ as determined in Ref. 23 that reports measurements down to $q_{\min}^{\text{Hux}} = 0.03 \text{ \AA}^{-1}$ denoted by the dashed-dotted line. The blue line is a guide to the eye.

class³². Further, $\chi(q)\Gamma_q$ is approximately constant as a function of q down to q^0 highlighting that the underlying spin fluctuations are localized in real space. In contrast, the dynamical exponent $z = 5/2$ and $\chi(q)\Gamma_q \rightarrow 0$ for $q \rightarrow 0$ observed below the crossover value q^0 , are characteristic of itinerant spin fluctuations. Because the contribution of the conduction electrons to the total ordered moment is less than 3%³³, below T_C fluctuations of localized f magnetic moments are dominant. Spin fluctuations with a dual character are consistent with the moderately enhanced Sommerfeld coefficient $\gamma = 34 \text{ mJ/K}^2$ mol of UGe₂^{46,47} and a next-nearest-neighbor uranium distance $d_{\text{U-U}} = 3.85 \text{ \AA}$ ⁴⁸ near to the Hill value of 3.5 \AA ⁴⁹ that both suggest that the $5f$ electrons in UGe₂ are hybridized with the conduction electrons.

In conclusion, the dual nature of spin fluctuations revealed by our MIEZE measurements strongly supports the scenario of p-wave superconductivity in UGe₂. First, to promote strong longitudinal fluctuations requires strong Ising anisotropy that typically is a result of localized f electrons with substantial spin-orbit coupling, and is consistent with critical Ising exponents that we observe above q^0 . Second, the theory for p-wave pairing assumes that it is the *same* itinerant electrons that are responsible for the coexisting FM and superconducting states²², highlighting that the low-energy itinerant spin fluctuations below q^0 discovered here are crucial to mediate p-wave superconductivity. The maximum superconducting critical temperature T_s occurs at the QPT at p_x ^{20,21}. Here a substantial increase of the Sommerfeld coefficient⁵⁰ and changes in the electronic structure observed near p_x ^{51,52} suggest that the hybridization of $5f$ electrons and conduction electrons increases at p_x and corroborates that spin fluctuations with a dual nature are relevant for p-wave superconductivity. This is supported by a theory based on competition of FM exchange and the Kondo interaction that results in a localized to itinerant transition at p_x ^{53,54}.

Further, we note that our findings of longitudinal critical fluctuations in UGe_2 are also consistent with the findings for UCoGe ⁵⁵, which is another material that is a candidate for p-wave superconductivity. However, the results on UCoGe by Hattori *et al.*⁵⁵ were obtained by NMR measurements that are unable to probe spin fluctuations at finite q and, in turn, are unable to observe an itinerant-to-localized crossover as we report it here. Similarly, TAS measurements of UCoGe by Stock *et al.*⁵⁶ lack the required momentum and energy transfer resolution.

Finally, we note that the crossover value q^0 corresponds to a length scale of approximately 160 Å. The superconducting coherence length of UGe_2 was estimated as $\xi^{\text{SC}} = 200 \text{ \AA}^{20}$, which shows that the spin fluctuations relevant to the p-wave pairing are present at $q < q^0$. This may explain why triple-axis measurements of the spin fluctuation near p_x with limited resolution were inconclusive⁵⁷. Although, the pressure dependence of the crossover length scale q^0 remains to be determined to unambiguously associate it with the unconventional superconducting state in UGe_2 , our results highlight that recent developments in ultra-high resolution neutron spectroscopy are critical for the study of low-energy spin fluctuations that are believed to drive the emergence of quantum matter states. Here the fluctuations that appear at zero q such as for ferromagnetic and electronic-nematic quantum states can immediately be investigated via the MIEZE SANS configuration used here. In addition, MIEZE can be extended in straightforward fashion to study quantum fluctuations arising

at large q ⁵⁸, allowing for insights in antiferromagnetic QPTs and topological forms of order.

ACKNOWLEDGMENTS

The authors wish to thank the technical staff at MLZ for their help in conducting the experiments. We are grateful to Björn Pedersen for assistance with the neutron Laue diffraction measurements. We also acknowledge useful discussions with J. M. Lawrence, F. Ronning, and P. Böni. Work at Los Alamos National Laboratory (LANL) was supported by LANL Laboratory Directed Research and Development program. Work at Technische Universität München was supported by the TRR80 Project F2. The authors acknowledge the financial support by the Federal Ministry of Education and Research of Germany in the framework of 'Longitudinale Resonante Neutronen Spin-Echo Spektroskopie mit Extremer Energie-Auflösung' (project number 05K16WO6). The work by FH and MJ was supported through a Hans Fischer fellowship of the Technische Universität München — Institute for Advanced Study, funded by the German Excellence Initiative and the European Union Seventh Framework Programme under grant agreement n° 291763. CP acknowledges financial support through ERC AdG ExQuiSid (788031) and DGF FOR960 (project 4). We also acknowledge support from the European Union through the Marie-Curie COFUND program.

* Current address: Division of Materials Sciences and Engineering, Ames Laboratory, U.S. DOE, Iowa State University, Ames, Iowa 50011, USA

† Corresponding Author: marc.janoschek@psi.ch

¹ T.-H. Han, J. S. Helton, S. Chu, D. G. Nocera, J. A. Rodriguez-Rivera, C. Broholm, and Y. S. Lee, *Nature* **492**, 406–410 (2012).

² R. M. Fernandes, A. V. Chubukov, and J. Schmalian, *Nature Physics* **10**, 97–104 (2014).

³ D. J. Scalapino, *Rev. Mod. Phys.* **84**, 1383 (2012).

⁴ S. Mühlbauer, B. Binz, F. Jonietz, C. Pfleiderer, A. Rosch, A. Neubauer, R. Georgii, P. Böni, *Science* **323**, 915-919 (2009).

⁵ M. Janoschek, M. Garst, A. Bauer, P. Krautscheid, R. Georgii, P. Böni, and C. Pfleiderer, *Phys. Rev B* **87**, 134407 (2013).

⁶ M. C. Aronson, R. Osborn, R. A. Robinson, J. W. Lynn, R. Chau, C. L. Seaman, and M. B. Maple, *Phys. Rev. Lett.* **75**, 725 (1995).

⁷ A. Schröder, G. Aeppli, R. Coldea, M. Adams, O. Stockert, H.v. Löhneysen, E. Bucher, R. Ramazashvili, and P. Coleman, *Nature* **407**, 351–355 (2000).

⁸ H. Kadowaki, Y. Tabata, M. Sato, N. Aso, S. Raymond, and S. Kawarazaki, *Phys. Rev. Lett.* **96**, 016401 (2006).

⁹ W. Knafo, S. Raymond, P. Lejay and J. Flouquet, *Nature Physics* **5** 753–757 (2009).

¹⁰ A. M. Tsvelik, *Quantum Field Theory in Condensed Matter Physics*, Cambridge University Press, (2003).

¹¹ E. Dagotto, *Science* **309**, 257 (2005).

¹² C. Pfleiderer, *Rev. Mod. Phys.* **81**, 1551 (2009).

¹³ K. T. Moore and G. van der Laan, *Rev. Mod. Phys.* **81** 235 (2009).

¹⁴ H. J. Im, T. Ito, H.-D. Kim, S. Kimura, K. E. Lee, J. B. Hong, Y. S. Kwon, A. Yasui, and H. Yamagami, *Phys. Rev. Lett.* **100**, 176402

(2008)

¹⁵ A. R. Schmidt, M. H. Hamidian, P. Wahl, F. Meier, A. V. Balatsky, J. D. Garrett, T. J. Williams, G. M. Luke, and J. C. Davis, *Nature* **465**, 570 (2010).

¹⁶ N. P. Butch, M. E. Manley, J. R. Jeffries, M. Janoschek, K. Huang, M. B. Maple, A. H. Said, B. M. Leu, and J. W. Lynn, *Phys. Rev. B* **91**, 035128 (2015).

¹⁷ M. Janoschek, Pinaki Das, B. Chakrabarti, D. L. Abernathy, M. D. Lumsden, J. M. Lawrence, J. D. Thompson, G. H. Lander, J. N. Mitchell, S. Richmond, M. Ramos, F. Trouw, J.-X. Zhu, K. Haule, G. Kotliar, E. D. Bauer, *Science Advances* **1**, e1500188 (2015).

¹⁸ E. A. Goremychkin, H. Park, R. Osborn, S. Rosenkranz, J.-P. Castellan, V. R. Fanelli, A. D. Christianson, M. B. Stone, E. D. Bauer, K. J. McClellan, D. D. Byler, J. M. Lawrence, *Science* **359**, 186-191 (2018).

¹⁹ R. Gähler, R. Golub, and T. Keller, *Physica B* **180**, 899 (1992).

²⁰ S. S. Saxena, P. Agrwal, A. Ahilan, F. M. Grosche, R. K. W. Haselwimmer, M. J. Steiner, E. Pugh, I. R. Walker, S. R. Julian, P. Monthoux, G. G. Lonzarich, A. Huxley, I. Sheikhen, D. Braithwaite, and J. Flouquet, *Nature* **406**, 587 (2000).

²¹ C. Pfleiderer and A. D. Huxley, *Phys. Rev. Lett.* **89** 147005 (2002).

²² D. Fay and J. Appel, *Phys. Rev. B* **22**, 3173 (1980).

²³ A. D. Huxley, S. Raymond, and E. Ressouche, *Phys. Rev. Lett.* **91** 207201 (2003).

²⁴ P. Monthoux and G. G. Lonzarich, *Phys. Rev. B* **59** 14598 (1999).

²⁵ W. Häußler, B. Gohla-Neudecker, R. Schwikowski, D. Streibl and P. Böni, *Physica B* **397**, 112 (2007).

²⁶ J. Kindervater, N. Martin, W. Häußler, M. Krautloher, C. Fuchs, S. Mühlbauer, J.A. Lim, E. Blackburn, P. Böni, and C. Pfleiderer,

- EPJ Web of Conferences **83**, 03008 (2015).
- ²⁷ Ma. Krautloher, J. Kindervater, T. Keller, and W. Häubler, *Rev. Sci. Instr.* **87**, 125110 (2016).
- ²⁸ See Supplemental Material at <http://link.aps.org/supplemental/10.1103/PhysRevB.000.000000> for the characterization of the sample with neutron Laue diffraction and neutron depolarization analysis, as well as detailed information about the used MIEZE setup, and additional SANS measurements. Further, we describe approximations used for the analysis of energy-integrated magnetic critical scattering and resolution calculations. Finally, we explain how the MIEZE data was analyzed.
- ²⁹ N. T. Huy *et al.*, *J. Magn. Magn. Mater.* **321**, 2691 (2009).
- ³⁰ J.W. Lynn, L. Vasiliu-Doloc, and M.A. Subramanian, *Phys. Rev. Lett.* **80**, 4582 (1998).
- ³¹ Ch. Simon, S. Mercone, N. Guiblin, C. Martin, A. Brulet, and G. Andre, *Phys. Rev. Lett.* **89**, 207202 (2002).
- ³² P. M. Chaikin and T. C. Lubensky, *Principles of Condensed Matter Physics*, Cambridge University Press (1995).
- ³³ N. Kernavanois, B. Grenier, A. Huxley, E. Ressouche, J. P. Sanchez, and J. Flouquet *Phys. Rev. B* **64**, 174509 (2001).
- ³⁴ W. Marshall and R. D. Lowde, *Rep. Prog. Phys.* **31** 705 (1968).
- ³⁵ G. L. Squires, *Introduction to the theory of thermal neutron scattering*, Dover Publications (1978).
- ³⁶ P. C. Hohenberg and B. I. Halperin, *Rev. Mod Phys.*, **49** 435 (1977).
- ³⁷ J. Kindervater, S. Säubert, and P. Böni, *Phys. Rev. B* **95**, 014429 (2017).
- ³⁸ V. J. Minkiewicz, M. F. Collins, R. Nathans, and G. Shirane *Phys. Rev.* **182**, 624 (1969).
- ³⁹ C. J. Glizka, V. J. Minkiewicz, and L. Passell, *Phys. Rev. B* **16**, 4084 (1977).
- ⁴⁰ O. W. Dietrich, J. Als-Nielsen, and L. Passell, *Phys. Rev. B* **14**, 4923 (1976).
- ⁴¹ B. I. Halperin and P. C. Hohenberg, *Phys. Rev.* **177**, 952 (1969).
- ⁴² G.G. Lonzarich, *J. Magn. Magn. Mater.* **54–57**, 612 (1986).
- ⁴³ N. Bernhoeft, S. A. Law, G. G. Lonzarich, and D. McK. Paul, *Phys. Scr.* **38**, 191 (1988).
- ⁴⁴ G.G. Lonzarich, L.Taillefer, *J. Phys. C* **18**, 4339 (1985).
- ⁴⁵ G. G. Lonzarich, *Electron: A Centenary Volume*, edited by M. Springford, Cambridge University Press (1999), p. 109.
- ⁴⁶ J.C.Lashley, R.A.Fisher, J.Flouquet, F.Hardy, A.Huxley, N.E. Phillips, *Physica B* **378–380** 961-962 (2006).
- ⁴⁷ R. Troć, Z. Gajek, and A. Pikul, *Phys. Rev. B* **86**, 224403 (2012).
- ⁴⁸ K. Oikawa, T. Kamiyama, H. Asano, Y. Ōnuki, and M Kohgi, *J. Phys. Soc. Jpn.* **65** 3229 (1996).
- ⁴⁹ H. H. Hill, *Plutonium and other Actinides*, edited by W. N. Miner, The Metallurgical Society of AIME, New York (1970).
- ⁵⁰ N. Tateiwa, T. C. Kobayashi, K. Amaya, Y. Haga, R. Settai, and Y. Ōnuki, *Phys Rev B* **69** 180513 (2004).
- ⁵¹ T. Terashima, T. Matsumoto, C. Terakura, S. Uji, N. Kimura, M. Endo, T. Komatsubara, and H. Aoki, *Phys. Rev. Lett.* **87**, 166401 (2001).
- ⁵² R. Settai M. Nakashima, S. Araki, Y. Haga., T. C. Kobayashi, N. Tateiwa, H. Yamagami, and Y. Onuki, *J. Phys.: Condens. Matter* **14** L29–L36 (2002).
- ⁵³ C. Thomas, A. S. da Rosa Simões, J. R. Iglesias, C. Lacroix, N. B. Perkins, and B. Coqblin, *Phys. Rev. B*, **83** 014415 (2011).
- ⁵⁴ S. Hoshino and Y. Kuramoto, *Phys. Rev. Lett.*, **111** 026401, (2013).
- ⁵⁵ T. Hattori, Y. Ihara, Y. Nakai, K. Ishida, Y. Tada, S. Fujimoto, N. Kawakami, E. Osaki, K. Deguchi, N. K. Sato, and I. Satoh, *Phys. Rev. Lett.* **108**, 066403 (2012).
- ⁵⁶ C. Stock, D. A. Sokolov, P. Bourges, P. H. Tobash, K. Gofryk, F. Ronning, E. D. Bauer, K. C. Rule, and A. D. Huxley, *Phys. Rev. Lett.* **107**, 187202 (2011).
- ⁵⁷ M. W. Képa, D. A. Sokolov, M Böhm and A. D. Huxley, *J. Phys.: Conf. Ser.* **568** 042016 (2014).
- ⁵⁸ N. Martin, *Nuclear Inst. and Methods in Physics Research*, A **882** 11–16 (2018).